Methane hydrate recycling offshore of Mauritania probably after the last glacial maximum

Ang Li [a*], Richard J. Davies [b], Simon Mathias [a]

[a] Centre for Research into Earth Energy Systems (CeREES), Department of Earth Sciences, Science Labs, Durham University, DH1 3LE, UK

[b] School of Civil Engineering and Geosciences, Newcastle University, Newcastle upon Tyne, Tyne and Wear, NE1 7RU, UK

Corresponding author: Tel: +44 7842739999 E-mail: happyleon2009@gmail.com

Abstract: To what extent methane liberated from marine hydrate will enter the ocean during a warmer world is unknown. Although methane release due to hydrate dissociation has been modelled, it is unclear whether or not methane will reach the seafloor during a warmer world and therefore contribute to oceanic and atmospheric budgets. Here we show, using a new three-dimensional (3-D) seismic dataset, that some hydrate deposits surround the gas chimneys passing through the HSZ. Bottom water warming since the last glacial maximum (LGM) is interpreted to cause hydrate dissociation but critically some of the released methane was not vented to the ocean. The released gas caused seal failure and free gas entered the hydrate stability zone (HSZ) through vertical gas chimneys to where new hydrate accumulations formed. This process is a new evidence for methane recycling and could account in part for the lack of methane in ice core records that cover warming events during the late Quaternary. This research provides new insight into how methane could be recycled rather than vented during a warmer world.

Key words: gas hydrate, gas chimney, BSR, methane recycling

1 Introduction

Methane is a potent greenhouse gas and vast quantities of it are locked-up in marine hydrate along the continental margins (Kvenvolden, 1993). Methane released from hydrate could have a role in accelerated climatic warming, ocean acidification and de-oxygenation (Biastoch et al., 2011; Dickens, 2003). There is already potential evidence, such as plumes of gas bubbles, for methane liberated from hydrates venting into the ocean due to oceanic

warming in the Arctic (Westbrook et al., 2009) and along the US Atlantic margin (Phrampus and Hornbach, 2012; Skarke et al., 2014). But isotopic records that cover rapid Quaternary climate change events from ice cores of polar region indicate that methane from hydrate is not released during periods of rapid warming (Sowers, 2006). Methane stored in hydrate is probably a contributor rather than the main source of atmospheric methane budget after the last glacial maximum (LGM, Chappellaz et al., 1993). The fundamental question of whether large amount of methane from hydrate escapes into oceans and the atmosphere remains unanswered. If it did not reach the seabed, how is methane retained in the subsurface?

Hydrates are usually identified in marine settings through the identification of bottom simulating reflectors (BSRs) in seismic reflection datasets. BSRs mark the base of the hydrate stability zone (BHSZ) below which free gas is often trapped and this configuration yields a medium to high acoustic impedance contrast (Shipley et al., 1979). As the water depth shallows at continental margins, the BSR also shoals and seismic imaging sometimes shows examples of it intersecting the seabed at a water depth between ~350 and ~600 m (Boswell and Collett, 2011). In general the ascent of methane into the hydrate stability zone (HSZ) should be impeded, as hydrates clogs interconnected pores and fractures (Nimblett and Ruppel, 2003). But methane can sometimes pass through the HSZ and arrive at the seabed (Liu and Flemings, 2006). Seismic evidence for this methane venting is often gas chimneys with pockmark at the seabed and they are thought to represent the occurrence of vertical migration of pore fluid (Hovland and Judd, 1988; Cartwright and Santamarina, 2015).

Venting into the atmosphere is not necessarily the fate of gas that has been liberated from methane hydrate. Methane could be recycled to the BHSZ (Davies and Clarke, 2010; Paull et al., 1994), dissolved into the ocean and replaced by other gases such as oxygen during its ascent (McGinnis et al., 2006) and oxidised aerobically in the shallow ocean (Ward et al., 1987) or anaerobically in the sub-seabed sediment (Hoehler et al., 2000). Using a new 3-D seismic survey offshore of Mauritania, we consider the fate of methane liberated due to oceanic warming since the LGM as a potential scenario for how marine hydrates will behave due to a future warmer world.

2 Geological setting

The area covered by the 3-D seismic survey is offshore of Mauritania (Fig. 1) where the water depth ranges from 50 to 1800 m (Fig. 1b). The shelf-slope break occurs at ~120 m water depth and the continental slope dips at ~3°. In the southeast of the survey there are a number of canyons that are part of the Cap Timiris Canyon system. The study area is located between two of these canyons and covers an area of ~23 km^2 and the uppermost ~100 m of the sedimentary succession. It is most likely dominated by the fine-grained hemi-pelagic sediment interbedded with turbidite mud and sand, deposited during alternating climatic periods of aridity and humidity in the Pleistocene and Holocene (Henrich et al., 2008; Zühlsdorff et al., 2007). The gravity cores of GeoB 8507-3 (Fig. 1a) record the uppermost 10 m-thick sediments in the Timiris Canyon and show that the sedimentation rate averages at 190 m/my (metres per million years) in the Holocene (Zühlsdorff et al., 2007), but this rate may not be typical in the study area. This rate can be up to 685 m/my in the records of GeoB 8509-2 (Zühlsdorff et al., 2007). The commercial wells, Ras Al Baida-1 and Al Kinz-1, show that there are traces of hydrocarbons throughout late Cretaceous and Paleogene sediments (Vear, 2005). Gas migration in the marine hydrate system has been documented in the area covered by another 3-D seismic survey offshore of Mauritania, which is ~130 km to the south of the study area (Davies et al., 2012; Yang and Davies, 2013; Yang et al., 2013; Davies et al., 2014).

3 Seismic data and methodology

The 3-D seismic data cover an area of ~3800 km^2. The bin spacing is 12.5 m × 25 m. The recording is cut by a frequency filter of 3 – 200 Hz. The dominant frequency in the upper 100 m-thick sediment is 55 Hz. These data have a sampling rate of 2 ms and are zero-phased. They are displayed in the depth domain after being Kirchoff depth migrated. The velocity model for this migration is not provided in this research. A positive polarity is defined by a peak on the seismic trace and displayed by a black-red-black seismic loop on the cross section, which represents an increase in the acoustic impedance. The extracted seismic attributes include RMS (root mean square) amplitude and dip-magnitude. The maps of these

attributes are utilised to pinpoint the hydrate/gas and visualise the migration-related features (e.g. pockmarks) in an area of interest.

The BSR is picked along the troughs of the seismic traces that together produce a reflection usually cross-cutting the stratal reflections. At the places where this cross-cutting cannot be identified the BSR depth is inferred by linear interpolation or consistent with the high-amplitude, horizon-parallel reflection. A numerical model for 2-D heat conduction is used to simulate the location of the present BHSZ (appendix) and validate the interpretation of the BSR.

4 Observations

4.1 Seabed and BSR

The seabed dips to the southwest and only one pockmark (~200 m in diameter) is found to the northeast of the landward terminus of the BSR (Fig. 1b). No seabed amplitude anomaly can be seen in or near this pockmark, indicating the absence of the carbonate crust that has been documented at venting sites (e.g. Hovland et al., 1987). The BSR is observable over most of the region at the water depths of 750 – 1300 m, dipping at ~4° and deepening southwestern. On a seismic profile it is characterised by a negative high-amplitude reflection and cross-cutting stratal reflections at low angles (<5°) (Fig. 2). The BSR does not intersect with the seabed reflection. Instead, it often terminates at ~70 mbsf (metres below the seafloor) (Fig. 2a). The seabed intersection depth (SID) is estimated by the numerical model of heat conduction to be 711 m (Fig. A.1, appendix), though at some sites outside the study area we observe that the SID is ~740 m.

4.2 Seismic chimneys and high-amplitude anomalies

4.2.1 Seismic chimneys

15 seismic chimneys have been identified in the study area. They are 130 – 180 m in height, 80 – 200 m in diameter and characterised by vertically aligned discontinuities in seismic reflections (Fig. 3). The discontinuity takes the form of a localised, sub-circular region of positive relief at each reflection above the BSR. The relief is 5 – 10 m and the

diameter of the regions of positive relief maximises at the reflections D and E (Fig. 4). Apart from the reflections near to the top of the gas chimney (e.g. reflection B, Fig. 3, 4), those inside the chimneys have lower amplitude than surrounding reflections. The observations are similar to gas chimneys identified offshore mid-Norway (Hustoft et al, 2010). The bases of the gas chimneys are identified on the basis of where reflections show no deflection. We also see that the alignment of the bases is sub-parallel to the present BSR. The root zone is 30 – 70 m below the present BSR (Fig. 3). Their tops are located at the reflection immediately below the seabed but there is no evidence, such as pockmarks, for their presence at the current seabed (Fig. 3). The chimneys are most unlikely to be the velocity pull-up artefacts. Such artefacts are characterised by distorted reflections or obscure imaging vertically below the anomalous velocity unit, while in this case the reflections in the deep subsurface are intact and show no difference with the nearby reflections (Fig. 3).

4.2.2 High-amplitude anomalies

Around the seismic chimneys, but only detected by mapping certain reflections (D and E, Fig. 3c) are sub-circular, sub-elliptical or irregularly shaped high amplitude anomalies that have the same polarity with the seabed (Fig. 3 and 4). We term these 'positive high-amplitude anomalies' (PHAAs). They are ~70 m below the seabed and ~2.4 km away from the termination of the BSR in the seaward direction. Chimney 10 for example, is surrounded by three regions of high amplitude, each with an irregular geometry. The high-amplitude values among these regions occur closest to the chimney (Fig. 4). The isolated PHAA adjacent to chimney 7 covers an area of ~0.08 km^2 and has a sub-elliptical geometry. Its long axis is sub-parallel to the dip of the continental slope. The amplitude values of this PHAA are largest near the gas chimney and diminish progressively along the reflections towards its periphery. In plan-view, chimney 7 is not in the centre of the PHAA. A third example has two associated chimneys (8 and 12, Fig. 4). They both are surrounded by PHAAs which coalesce to form a larger PHAA with an area of 0.21 km^2. Again in plan form these two chimneys are not central to their respective PHAAs (Fig. 4).

5 Interpretation

5.1 Gas trapped below the BSR

The amplitude map of the BSR shows a set of high-amplitude bands (Fig. 2). Similar bands have been identified before offshore of Mauritania (Li et al. 2016). In both examples they have the opposite polarity to the seabed (Fig. 2a), suggesting a decrease in acoustic impedance. There are also multiple phase reversals along the BSR (Fig. 2a, c). They occur at the edge of the band, where we predict the pores of the thin beds are filled with hydrate above the BSR and gas below it, producing high and low acoustic impedance, respectively (Fig. 2c). The transition of the seismic phase in a step-like pattern in space causes the aligned high-amplitude termination along the BSR. This configuration coincides with the other known marine hydrate systems (e.g. Bünz and Mienert, 2004).

Representative seismic lines where these enhanced reflections are present show that the gas chimneys root into a zone below the BSR (marked FGZ on Fig. 3). This spatial relationship, coupled with the knowledge that the gas chimneys are probably a migration pathway for pore fluid (Cartwright and Santamarina, 2015) implies that free gas trapped below the BSR was transported to the shallower subsurface. Because there is no evidence for pockmarks or indeed any other morphological features at the seabed we propose there was no significant escape of methane into the ocean. Therefore, similar to Ivanov et al. (2007), the gas chimneys did not intersect a free surface.

5.2 Hydrate deposits

The PHAAs are interpreted to be primarily caused by gas hydrate deposits that have a higher P-wave velocity, probably between 3760 – 4000 m/s (Sloan and Koh, 2008), than that of the seawater-filled background sediment. A high hydrate saturation (e.g. >35%, Hornbach et al., 2003) can increase the acoustic impedance of hydrate-filled sediment to the level such that should be detected on seismic dataset. The thickness of the PHAAs is estimated to be up to ~16 m at the seismic scale based on the vertical resolution of ~8 m (the P-wave velocity of the seawater-filled sediment is assumed to be 1800 m/s and the vertical resolution is one quarter of the wavelength). But gravity cores sampled at the Timiris Canyon indicate the

thickness of sands is likely to be no more than 10 m (Zühlsdorff et al., 2007). Therefore, we think the PHAA is the seismic response to one or more than one hydrate-containing porous sands.

We propose the hydrate accumulations were sourced from free gas transported through the gas chimneys. Methane carried within pore fluid migrated through the fractures and then flowed laterally along permeable beds in an up dip direction where hydrate would have formed around the chimney point source (Davies et al., 2014; Xu and Ruppel, 1999). As the PHAAs are discrete regions surrounded by lower seismic amplitudes, our preferred interpretation is that hydrate at this level was absent or at a low concentration before the chimneys formed and fed the new hydrate accumulations.

Our interpretation suggests that the geometry of the PHAA is the result of methane migration after leaving the gas chimneys. Given that the pore fluid could form a frictionless buoyant gravity current, its spreading out will be a function of the time, the density difference, the input flux and the effective permeability of the porous medium (Lyle et al., 2005). As the base of the dipping cap rock can be considered as an inclined plane and there is a density contrast between free gas and seawater, the buoyancy has a role in driving the fluid migrating up dip, which leads to the ellipsoidal geometry of the PHAA elongated in the direction that is parallel to the dip of the continental margin (Vella and Huppert, 2006). Such a pattern of migration has been seen in the Sleipner field of the North Sea, where CO_2 has been injected into subsurface sands. The geometry of the CO_2 reservoir can be detected by the seismic imaging that displays a comparable high amplitude zone (Boait et al., 2012). Another example of this geometry is lateral migration of gas along the BHSZ offshore of Mauritania, in which case tear-drop shaped high amplitudes that loop around and envelope point-source gas chimney have been imaged (Davies et al., 2014).

It cannot be completely ruled out that the PHAAs are the seismic response to the authigenic carbonate-cemented sediment. An example outcropping at the seabed was seen in the Gulf of Mexico (Roberts et al., 2006). The carbonate cements could form as a result of

anaerobic methane oxidation that develops in the methane-rich environment (Hovland et al., 1987). But the PHAAs, which are ~70 mbsf, may be too deep for this methane oxidation to take place as the sulfate-methane interface (SMI), which is at the base of the sulfate reduction zone, is normally at < 70 mbsf (Borowski et al., 1999).

6 Discussion

6.1 Methane passing through the HSZ

In general methane entering the HSZ will be trapped within it in some way or added to its base when the base of HSZ deepens, but free gas can also exist within or pass through the HSZ. Some hypotheses have been proposed to explain this phenomenon. (a) Once gas enters the HSZ, it will form hydrates, depleting pore water and therefore increasing its salinity (Liu and Flemings, 2006). Furthermore, the hydrate clogging slows the removal of the highly concentrated ionised salt (Milkov et al., 2004). The resulting hypersaline pore environment will inhibit further hydration (Sloan and Koh, 2008) and this will allow gas for some time to pass by (Liu and Flemings, 2006; Liu and Flemings, 2007). (b) Excessive methane may consume all in-situ water to form hydrate, which will create a water-free environment in the low-permeability sediment without no more gas being trapped (Tréhu et al., 2004). In this case all the water can be depleted when the methane accounts for >70.8% of the total volume of pore fluid under in-situ conditions (pore water is assumed to be initially saturated with methane and the height of the water column above the site is assumed to be 950 m). (c) Where the chimney intersects with the BSR, the base of the HSZ is redefined by the vertical intrusion of the warm advecting fluid. The perturbation zone, which coincides with the outline of gas chimney, is physically stable for gas to exist (Wood et al., 2002). Here either one or any combination of these mechanisms may contribute to the process of gas passing through the HSZ.

6.2 Model

We interpret that the gas chimneys did not reach the modern seabed. The vertical distance between the tops of the gas chimneys and the seabed reflection cannot be clearly identified in the seismic dataset and is probably less than 8 m (vertical resolution). Given that

the sedimentation rate ranges from 190 m/my to 685 m/my (Zühlsdorff et al., 2007), the age of the gas chimneys is estimated to be up to 12 – 42 kyr. A prominent, millennial-scale warming event in the past 12 – 42 kyr is the global warming since the LGM that is interpreted to cause the upward shift of the BHSZ and hence the hydrate re-incorporation. The interpretation of this shift is consistent with those in offshore of Oregon (Bangs et al., 2005) and on the Cascadia margin (Musgrave et al., 2006). To probe into how this hydrate re-incorporation took place, we introduce the numerical modelling.

Here we developed a 2-D finite diffusive heat-flow model that allows us to propose how the hydrate deposit formed after the LGM (Fig. 5, appendix). The model output of the variation of the bottom water temperature (BWT, Bintanja et al., 2008) and the relative sea level (RSL, Siddall et al., 2003) are taken as the input into this model to predict the shift of the BHSZ since the LGM. We assume that a) the marine sediments are isotropic and homogeneous, b) the pressure of pore fluid is hydrostatic and c) gases locked-up in hydrates are 100% methane. We determine the geothermal gradient by seeing whether the modelled BHSZ at steady state has a good match with its seismic observation (35 ^{o}C km^{-1}, appendix). The modelling results show that the BHSZ probably has shoaled by ~60 m since the LGM. Although this model affected by the uncertainty of the input data may not suffice to reveal what happened in the sutdy area (appendix), other researches, such as offshore of Oregon (Bangs et al., 2005), show that the upward shift of the BHSZ may be true at the places other than high-latitude zones. The thinning of the HSZ caused dissociation of the hydrate located at the BHSZ. The buoyancy of the released gas would have generated excess pore pressure that could have led to the development of hydraulic fractures (Xu and Germanovich, 2006). Therefore, the gas chimneys are interpreted to form during the period of rapid shallowing of the BHSZ, though the accurate timing of this formation is hard to determine. The hydrate started to accrete after the gas conduit was established between the sediments below the BHSZ and at the level of reflections D and E. Since then the hydrate accretion would continue as the BHSZ shoaled (Fig. 5). It is unlikely but cannot be ruled out entirely that the spatial relationship between the gas chimneys and the BSR is coincident.

6.3 Implications

The presence of the hydrate deposits implies that some of the gases released from hydrate since the LGM were recycled. We propose the sediments above the BHSZ prevent the escape of methane. The amount of methane recycled as hydrate can be amplified once this process has repeated at multiple horizons (e.g. Davies et al., 2014). But the volume of these accumulations is significantly lower than that of sediment that would have undergone dissociation after the LGM, which implies there are other mechanisms related to trapping and consuming methane. To our knowledge, they involve methane oxidisation (Treude and Ziebis, 2010), being trapped stratigraphically in situ, or recycled as new hydrate at the base (Davies and Clarke, 2010; Paull et al., 1994). To what extent methane can be re-incorporated before reaching seabed is still a question to be answered. But this mechanism could account in part for why ice cores do not record methane from marine hydrate during episodes of rapid climatic warming.

7 Conclusions

We found some hydrate deposits at tens of metres above the BHSZ in a high-quality 3-D seismic survey offshore of Mauritania. They are interpreted to be a good example for the re-incorporation of methane into hydrate during oceanic warming after the last glacial maximum. The 2-D heat flow model shows that due to this warming the BHSZ could shoal by ~60 m. Methane released from hydrate entered the HSZ via vertical fractures and was recycled as marine hydrates. From this model we can say methane escape towards the seabed was buffered. This offers a new evidence of methane recycling that could in part explain why methane from marine hydrates is not thought to be a main contributor to the atmospheric budget.

Acknowledgements

We are grateful to the Chariot Oil & Gas for providing the seismic data and allowing publication of the current study. Durham University and the China Scholarship Council (CSC) are acknowledged for funding the research. We also thank the Landmark University Grant Program for providing the seismic interpretation software and necessary technical support.

We thank Christian Berndt, Nathan L. Bangs, Richard Hobbs and Jinxiu Yang for their constructive discussions. The IT staff in Durham University's Department of Earth Sciences, Dave Stevenson and Gary Wilkinson, are thanked for supporting and maintaining the Earth Imaging Laboratory (EIL).

Appendix: Two-dimensional heat diffusion model for the BHSZ shift

We developed a 2-D finite diffusive heat-flow model to show an event of the BHSZ shoaling since the LGM. The governing equation for 2-D heat diffusion model is found from:

$$\rho_b C_b \frac{\partial T}{\partial t} = k_x \frac{\partial^2 T}{\partial x^2} + k_z \frac{\partial^2 T}{\partial z^2} \quad \text{(A.1)}$$

where T[Θ] is the sediment temperature, x[L] and z[L] are the sediment length and depth below the seafloor respectively, ρ_b[ML^{-3}] is the sediment density, C_b[$L^2T^{-2}\Theta^{-1}$] is the specific heat capacity and t[T] is time. k_x[$MLT^{-3}\Theta^{-1}$] and k_z[$MLT^{-3}\Theta^{-1}$] are the sediment thermal conductivities in the horizontal and vertical direction, respectively. The subsurface sediment is assumed to be isotropic and homogeneous such that k_x=k_z. We assume the constant thermal conductivity of 1 W m^{-1} K^{-1}, an average bulk density of 2000 kg m^{-3}, which are consistent with the results recorded in the Global Heat Flow Database and the drilling data of Ras El Baida A-1, and a specific heat capacity of 2200 J K^{-1} kg^{-1} (Rempel and Buffett, 1997). All the gases trapped in hydrates are assumed to be methane and their molecular structure to be type I ($CH_4 \cdot 5.75H_2O$). If the temperature for hydrate equilibrium, T_c[Θ], is known, the pressure, P_c[$ML^{-1}T^{-2}$], can be determined from the empirical equation (Lu and Sultan, 2008):

$$P_c = \exp\big((C_s S + D_s)T_c\big) \exp(E_s S) F_s \quad \text{(A.2)}$$

where S[ML^{-3}] is the salinity of pore fluid (35 ‰), equal to that of seawater. C_s[-], D_s[-], E_s[-] and F_s[-] are constants of 0.1711726397, 0.1046133676, -34.14836102 and 1.010769956×10^{-9}, respectively. We calculated the hydrostatic pressure gradient of 10.05 MPa/km by assuming the seawater density of 1024 kg m^{-3}.

Firstly we estimate the location of the present BHSZ and the geothermal gradient by using the numerical model that is discretised into 50 m (horizontal) × 10 m (vertical) cells

and subjected to the boundary conditions:

$$
\begin{array}{llll}
T = T_o, & 0 \le x \le 32 \text{ km}, & 600 \text{ m} \le z \le 2200 \text{ m}, & t = 0 \\
\partial T/\partial z = J, & 0 \le x \le 32 \text{ km}, & z = 2200 \text{ m}, & t > 0 \\
\partial T/\partial z = 0, & 0 \le x \le 32 \text{ km}, & z = 600 \text{ m}, & t > 0 \\
\partial T/\partial x = 0, & x = 32 \text{ km}, & 600 \text{ m} \le z \le 2200 \text{ m}, & t > 0 \\
\partial T/\partial x = 0, & x = 0, & 600 \text{ m} \le z \le 2200 \text{ m}, & t > 0
\end{array}
$$

where $J[\Theta L^{-1}]$ is the geothermal gradient, $T_o[\Theta]$ is the calculated ocean temperature in December 2009 (acquisition time of seismic data). The temperature of ocean water at each depth (results are shown in Fig. A.1) is the average of the values over the region 18-22^o N, 17-21^o W in December 2009, taken from the World Ocean Database (WOD). The geothermal gradient in the study area is unknown and two values of 29 ^{o}C km^{-1} (Davies et al., 2012) and 46 ^{o}C km^{-1} (measured at V29-124 (20.07^o N, 19.98^o W) in a Ewing-type probe, data from Global Heat Flow Database) recorded near the site are taken as the end-members to estimate the range of the BHSZ location. Some arbitrary values of the geothermal gradient (integers between 29 and 46 ^{o}C km^{-1}, not all the modelling results are shown) are also used to determine its value based on the seismic observation. Fig. A.1 shows that at time zero the observed BSR is within its predicted zone and the geothermal gradient of 35 ^{o}C km^{-1} has the modelling result that fits most with the observed BSR. The discrepancy between the observed and modelled BSR at the depths smaller than 1400 mbsf could be attributed to the subsurface temperature regime that does not reach the steady state (c.f. Phrampus and Hornbach, 2012). It can also be caused by the uncertainties in salinity and gas composition. The salinity increase of pore fluid from 35 ‰ to 40 ‰, which may happen during hydrate formation (Liu and Flemings, 2007), can shallow the depth of the BHSZ by 5.9 – 12.5 m in the model (not shown in Fig. A.1). The base of hydrates hosting 95% methane and 5% ethane is ~40 m shallower than that of hydrates comprising pure methane when the salinity of pore water is zero (equation for gas hydrate phase equilibrium is from Lu and Sultan, 2008). The geothermal gradient can be better constrained by the known salinity of pore fluid and the composition of gas trapped in hydrates, but to our knowledge they have not been documented before in the study area.

Next we use the numerical model to show the variation of the BHSZ since the LGM and to accelerate computing we narrow the modelled region. The model is changed to have a 400 × 200 cell temperature grid (with 20 m × 3.5 m cell dimensions). The initial and boundary condition can be written as:

$$
\begin{aligned}
&T = T_o', && 0 \le x \le 8 \text{ km}, && 600 \text{ m} \le z \le 1300 \text{ m}, && t = 0\\
&\partial T/\partial z = J, && 0 \le x \le 8 \text{ km}, && z = 1300 \text{ m}, && t > 0\\
&\partial T/\partial z = 0, && 0 \le x \le 8 \text{ km}, && z = 600 \text{ m}, && t > 0\\
&\partial T/\partial x = 0, && x = 8 \text{ km}, && 600 \text{ m} \le z \le 1300 \text{ m} && t > 0\\
&\partial T/\partial x = 0, && x = 0, && 600 \text{ m} \le z \le 1300 \text{ m} && t > 0
\end{aligned}
$$

where $T_o'[\Theta]$ is the initial temperature at 20 kyr ago. The bathymetry is from Fig. 2a and assumed to be unchanged since 20 kyr ago. The parameters of physical properties are shown in the table A.1. The data of RSL in the past 20 kyr are acquired by linearly interpolation from fig.1 by Siddall et al. (2003) (Fig. A.2a). We use the temperature anomalies in Bintanja et al. (2008), which were measured by marine oxygen isotope ratio ($\delta^{18}O$) records, to estimate the variation of the temperature of deep ocean with time (Fig. A.2b). Heat transfer and time during hydrate formation and dissociation are not considered. At each time step the reference frame of the vertical shift of the BHSZ is the seabed. Eq. A.1 is discretised in space using finite differences and then solved using the MATLAB ordinary differential equation (ODE) solver, ODE15s. Time-steps are chosen using the adaptive time-stepping functionality of ODE15s.

Fig. A.2c shows the BHSZ shoaled in the past 20 kyr at the site where the water depth is 825 m (its location is marked by the red triangle in Fig. 5). However, there are uncertainties in the modelling and some of them stem from the input values of parameters. Results based on different data show different degrees of oceanic warming, such as the data from the Paleoclimate Modelling Intercomparision Project Phase 3 (PMIP3, the data can be downloaded from https://pcmdi.llnl.gov/projects/esgf-llnl/) indicating that the temperature at the water depth of 600 – 900 m have increased by 0.8 – 3.9 ^{o}C since 20 kyr ago. The data of BWT and RSL are not directly measured offshore of Mauritainia and may not suffice to reveal what happened in the sutdy area.

Table A.1 Parameters of physical properties used in this model

Parameter	Value
Seawater density	1024 kg m^{-3}
Sediment density (ρ_b)	2000 kg m^{-3}
Specific heat capacity (C_b)	2200 J kg^{-1} K^{-1}
Thermal conductivity (k_x,k_z)	1 W m^{-1} K^{-1}
Geothermal gradient (J)	35 ^oC km^{-1}
Salinity of pore water (S)	35 ‰
Gas composition	100% CH_4
Molecular structure of clathrates	Type I

References

Bangs, N.L., Musgrave, R.J., and Tréhu, A.M., 2005, Upward shifts in the southern Hydrate Ridge gas hydrate stability zone following postglacial warming, offshore Oregon, *J. Geophys. Res.: Solid Earth (1978–2012)* **110**(B3).

Biastoch, A., Treude, T., Rüpke, L.H., Riebesell, U., Roth, C., Burwicz, E.B., Park, W., Latif, M., Böning, C.W., Madec, G. and Wallmann, K., 2011, Rising Arctic Ocean temperatures cause gas hydrate destabilization and ocean acidification, *Geophys. Res. Lett.* **38**(8).

Bintanja, R., and Van de Wal, R.S.W., 2008, North American ice-sheet dynamics and the onset of 100,000-year glacial cycles, *Nature* **454**(7206), 869-872.

Boait, F.C., White, N.J., Bickle, M.J., Chadwick, R.A., Neufeld, J.A., and Huppert, H.E., 2012, Spatial and temporal evolution of injected CO_2 at the Sleipner Field, North Sea, *J. Geophys. Res.* **117**, B03309.

Borowski, W.S., Paull, C.K., and Ussler, W., 1999, Global and local variations of interstitial sulfate gradients in deep-water, continental margin sediments: Sensitivity to underlying methane and gas hydrates, *Mar. Geol.* **159**(1), 131-154.

Boswell, R., and Collett, T.S., 2011, Current perspectives on gas hydrate resources, *Energy & environmental science* **4**(4), 1206-1215.

Bünz, S., and Mienert, J., 2004, Acoustic imaging of gas hydrate and free gas at the Storegga Slide. *J. Geophys. Res.: Solid Earth* **109**(B4).

Cartwright, J., and Santamarina, C., 2015, Seismic characteristics of fluid escape pipes in sedimentary basins: Implications for pipe genesis, *Mar. Pet. Geol.* **65**, 126-140.

Chappellaz, J.A., Fung, I.Y., and Thompson, A.M., 1993, The atmospheric CH_4 increase since the Last Glacial Maximum, *Tellus B* **45**(3), 228-241.

Davies, R.J., and Clarke, A.L., 2010, Methane recycling between hydrate and critically pressured stratigraphic traps, offshore Mauritania, *Geology* **38**(11), 963-966.

Davies, R.J., Thatcher, K.E., Mathias, S.A., and Yang, J., 2012, Deepwater canyons: An escape route for methane sealed by methane hydrate, *Earth Planet. Sci. Lett.* **323**, 72-78.

Davies, R.J., Yang, J., Hobbs, R., and Li, A., 2014, Probable patterns of gas flow and hydrate accretion at the base of the hydrate stability zone. *Geology* **42**(12), 1055-1058.

Dickens, G.R., 2003, Rethinking the global carbon cycle with a large, dynamic and microbially mediated gas hydrate capacitor, *Earth Planet. Sci. Lett.* **213**(3), 169-183.

Henrich, R., Hanebuth, T.J.J., Krastel, S., Neubert, N., and Wynn, R.B., 2008, Architecture and sediment dynamics of the Mauritania Slide Complex, *Mar. Pet. Geol.* **25**(1), 17-33.

Hoehler, T.M., Borowski, W.S., Alperin, M.J., Rodriguez, N.M., and Paull, C.K. ,2000, Model, stable isotope, and radiotracer characterization of anaerobic methane oxidation in gas hydrate-bearing sediments of the Blake Ridge. *In Proceedings of the Ocean Drilling Program, Scientific Results* (**164**, 79-85). Ocean Drilling Program College Station, TX.

Hornbach, M.J., Holbrook, W.S., Gorman, A.R., Hackwith, K.L., Lizarralde, D., and Pecher, I., 2003, Direct seismic detection of methane hydrate on the Blake Ridge, *Geophysics* **68**(1), 92-100.

Hovland, M., and Judd, A., 1988, *Seabed pockmarks and seepages: impact on geology, biology, and the marine environment*, Springer.

Hovland, M., Talbot, M.R., Qvale, H., Olaussen, S., and Aasberg, L, 1987, Methane-related Carbonate Cements in Pockmarks of the North Sea, *J. Sediment. Petrol.* **57**(5),

881-892.

Hustoft, S., Bünz, S., and Mienert, J., 2010, Three-dimensional seismic analysis of the morphology and spatial distribution of chimneys beneath the Nyegga pockmark field, offshore mid-Norway, *Basin Res.* **22**(4), 465-480.

Ivanov, M., Blinova, V., Kozlova, E., Westbrook, G.K., Mazzini, A., Minshull, T.A., and Nouzé, H., 2007, First sampling of gas hydrate from the Vøring Plateau. *Eos* **88**(19), 209-216.

Kvenvolden, K.A., 1993, Gas hydrates - geological perspective and global change, *Rev. Geophys.* **31**(2), 173-187.

Li, A., Davies, R.J. and Yang, J., 2016, Gas trapped below hydrate as a primer for submarine slope failures, *Mar. Geol.* **380**, 264-271.

Liu, X., and Flemings, P.B., 2006, Passing gas through the hydrate stability zone at southern Hydrate Ridge, offshore Oregon, *Earth Planet. Sci. Lett.* **241**(1), 211-226.

Liu, X., and Flemings, P.B., 2007, Dynamic multiphase flow model of hydrate formation in marine sediments, *J. Geophys. Res.: Solid Earth (1978–2012)* **112**(B3).

Lu, Z., and Sultan, N., 2008, Empirical expressions for gas hydrate stability law, its volume fraction and mass-density at temperatures 273.15 K to 290.15 K, *Geochemical Journal* **42**(2), 163-175.

Lyle, S., Huppert, H.E., Hallworth, M., Bickle, M., and Chadwick, A., 2005, Axisymmetric gravity currents in a porous medium, *J. Fluid Mech.* **543**, 293-302.

McGinnis, D.F., Greinert, J., Artemov, Y., Beaubien, S.E. and Wüest, A.N.D.A., 2006, Fate of rising methane bubbles in stratified waters: How much methane reaches the atmosphere?, *J. Geophys. Res.: Oceans* **111**(C9).

Milkov, A.V., Dickens, G.R., Claypool, G.E., Lee, Y.J., Borowski, W.S., Torres, M.E., Xu, W., Tomaru, H., Tréhu, A.M., and Schultheiss, P. ,2004, Co-existence of gas hydrate, free gas, and brine within the regional gas hydrate stability zone at Hydrate Ridge (Oregon margin): evidence from prolonged degassing of a pressurized core, *Earth Planet. Sci. Lett.* **222**(3), 829-843.

Musgrave, R.J., Bangs, N.L., Larrasoaña, J.C., Gràcia, E., Hollamby, J.A., and Vega, M.E., 2006, Rise of the base of the gas hydrate zone since the last glacial recorded by rock

magnetism. *Geology* **34**(2), 117-120.

Nimblett, J., and C. Ruppel, 2003, Permeability evolution during the formation of gas hydrates in marine sediments, *J. Geophys. Res.* **108**(B9), 2420.

Paull, C.K., Ussle, W., and Borowski, W.S., 1994, Sources of Biogenic Methane to Form Marine Gas Hydrates In Situ Production or Upward Migration? a. *Annals of the New York Academy of Sciences* **715**(1), 392-409.

Phrampus, B.J., and Hornbach, M.J., 2012, Recent changes to the Gulf Stream causing widespread gas hydrate destabilization. *Nature* **490**(7421), 527-530.

Rempel, A.W., and Buffett, B.A., 1997. Formation and accumulation of gas hydrate in porous media. *J. Geophys. Res.: Solid Earth* **102**(B5), 10151-10164.

Roberts, H.H., Hardage, B.A., Shedd, W.W., and Hunt Jr, J., 2006, Seafloor reflectivity—an important seismic property for interpreting fluid/gas expulsion geology and the presence of gas hydrate, *The Leading Edge* **25**(5), 620-628.

Shipley, T.H., Houston, M.H., Buffler, R.T., Shaub, F.J., McMillen, K.J., Ladd, J.W., and Worzel, J.L., 1979, Seismic evidence for widespread possible gas hydrate horizons on continental slopes and rises, *AAPG bulletin* **63**(12), 2204-2213.

Skarke, A., Ruppel, C., Kodis, M., Brothers, D., and Lobecker, E., 2014, Widespread methane leakage from the sea floor on the northern US Atlantic margin, *Nat.Geosci.***7**(9), 657-661.

Siddall, M., Rohling, E.J., Almogi-Labin, A., Hemleben, C., Meischner, D., Schmelzer, I., and Smeed, D. A., 2003, Sea-level fluctuations during the last glacial cycle, *Nature* **423**(6942), 853-858.

Sloan, E.D., and Koh, C.A., 2008, *Clathrate Hydrates of Natural Gases*, CRC Press.

Sowers, T., 2006, Late quaternary atmospheric CH_4 isotope record suggests marine clathrates are stable, *Science* **311**(5762), 838-840.

Tréhu, A.M., Flemings, P.B., Bangs, N.L., Chevallier, J., Gracia, E., Johnson, J.E., Liu, C.-S., Liu, X., Riedel, M., and Torres, M.E., 2004, Feeding methane vents and gas hydrate deposits at south Hydrate Ridge, *Geophys. Res. Lett.* **31**(23).

Treude, T., and Ziebis, W., 2010, Methane oxidation in permeable sediments at hydrocarbon seeps in the Santa Barbara Channel, California, *Biogeosciences (BG)* 7, 3095-3108.

Vear, A., 2005, Deep-water plays of the Mauritanian continental margin, *Petroleum Geology Conference Series* **6**, 1217–1232.

Vella, D., and Huppert, H.E., 2006, Gravity currents in a porous medium at an inclined plane, *J. Fluid Mech.* **555**, 353-362.

Ward, B.B., Kilpatrick, K.A., Novelli, P.C. and Scranton, M.I., 1987, Methane oxidation and methane fluxes in the ocean surface layer and deep anoxic waters. *Nature* **327**(6119), 226-229.

Westbrook, G.K., Thatcher, K.E., Rohling, E.J., Piotrowski, A.M., Pälike, H., Osborne, A.H., Nisbet, E.G., Minshull, T.A., Lanoisellé, M., James, R.H., and Hühnerbach, V., 2009, Escape of methane gas from the seabed along the West Spitsbergen continental margin. *Geophys. Res. Lett.* **36**(15).

Wood, W.T., Gettrust, J.F., Chapman, N.R., Spence, G. D., and Hyndman, R. D., 2002, Decreased stability of methane hydrates in marine sediments owing to phase-boundary roughness, *Nature* **420**(6916), 656-660.

Xu, W., and Germanovich, L.N. ,2006, Excess pore pressure resulting from methane hydrate dissociation in marine sediments: A theoretical approach, *J. Geophys. Res.: Solid Earth (1978–2012)*, **111**(B1).

Xu, W., and Ruppel, C., 1999, Predicting the occurrence, distribution, and evolution of methane gas hydrate in porous marine sediments, *J. Geophys. Res.: Solid Earth (1978–2012)* **104**(B3), 5081-5095.

Yang, J., and Davies, R.J., 2013, Gravity-driven faults: migration pathways for recycling gas after the dissociation of marine gas hydrates, *Mar. Geol.* **336**, 1-9.

Yang, J., Davies, R.J., and Huuse, M., 2013, Gas migration below gas hydrates controlled by mass transport complexes, offshore Mauritania, *Mar. Pet. Geol.***48**, 366-378.

Zühlsdorff, C., Wien, K., Stuut, J.-B.W., and Henrich, R., 2007, Late Quaternary sedimentation within a submarine channel–levee system offshore Cap Timiris, Mauritania, *Mar. Geol.* **240**(1), 217-234.

Figures

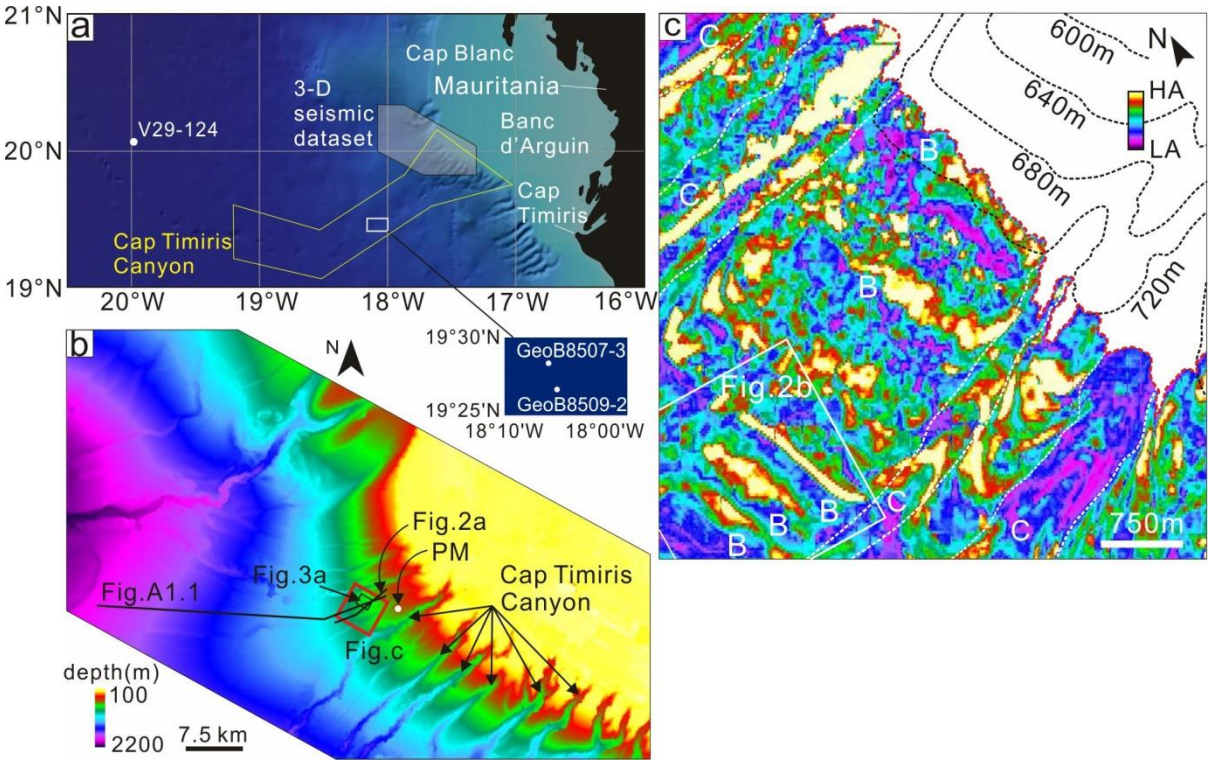

Fig.1 (a) Location of the 3-D seismic survey. The base map is from the online data provided by National Geophysical Data Centre (https://www.ngdc.noaa.gov/). Data of geothermal gradient and heat flow was measured at site V29-124 in 1977. (b) Bathymetric map showing the morphology of the seabed. Red box – study area. PM – pockmark. (c) The RMS amplitude map of the BSR in the study area. Red dashed line marks the landward extent of BSR and black dashed lines represent isobaths. The seismic features of bands (B) are interpreted in section 5.1. C – canyon, HA – high amplitude, LA – low amplitude in this and subsequent figures.

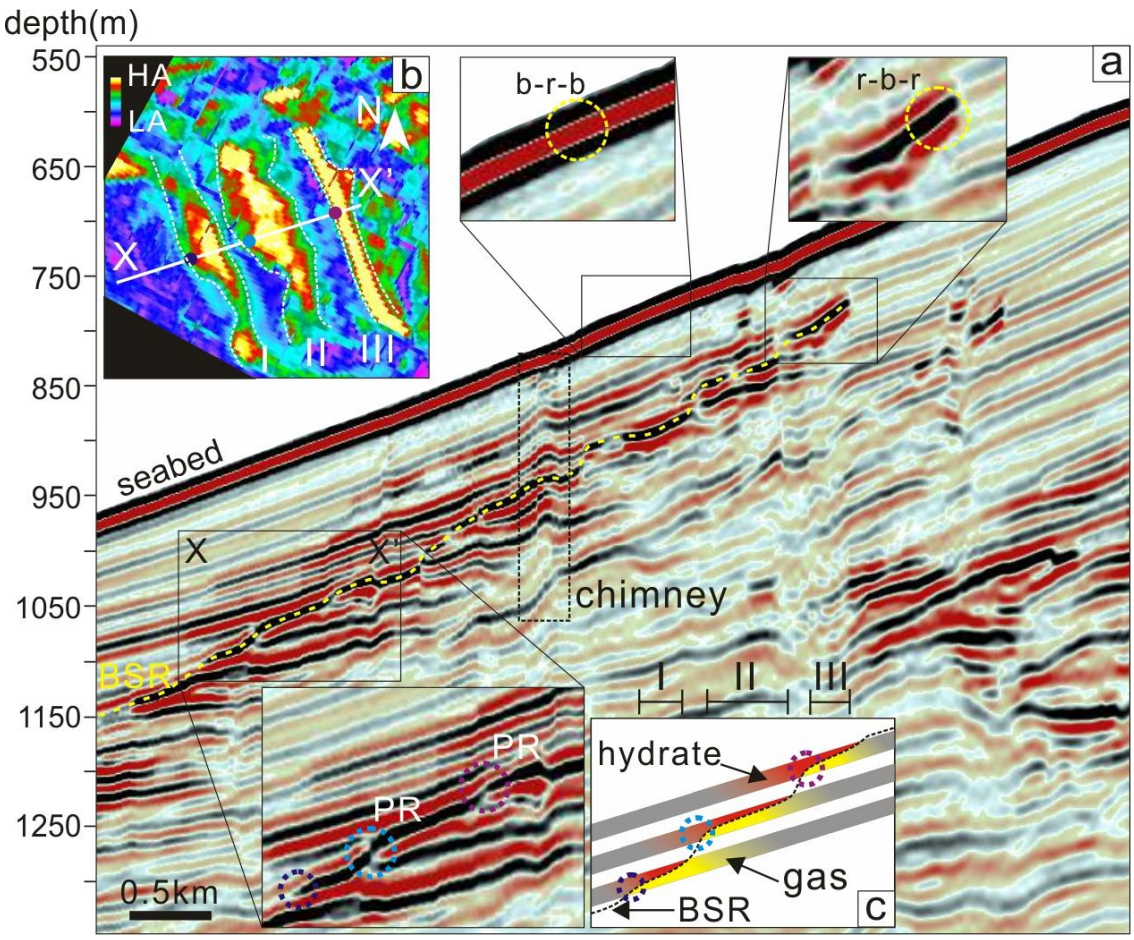

Fig.2 (a) A representative seismic section showing the typical features of a BSR and the gas accumulations sealed beneath it. B-r-b and r-b-r refer to the black-red-black and red-black-red seismic loop, respectively. (b) The RMS amplitude map of the BSR displaying three strike-parallel high amplitude bands (marked by I, II and III). (c) Interpretation of the cross section X-X'. At the seaward edge of the band feature, phase reversal sometimes can be seen. The grey colour represents a set of porous thin beds interbedded with less porous ones. The brighter red and yellow colours mark the higher saturation of hydrate and gas, respectively. PR – phase reversal.

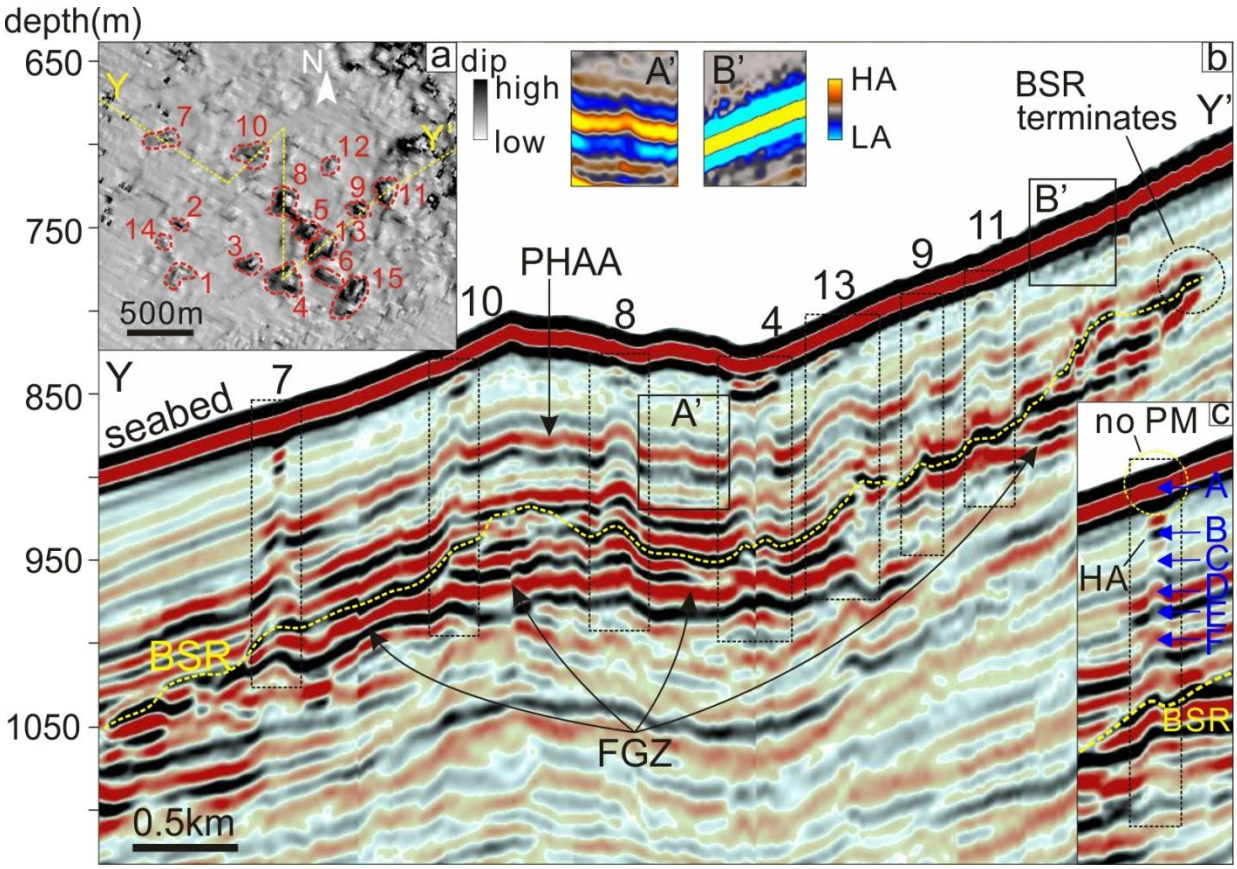

Fig.3 (a) Dip magnitude map of the reflection D. Its depth is marked in Fig. 3c. In plan view the positive relief of the chimney is marked in the darker colour. (b) A seismic section revealing the spatial location of some seismic chimneys. They are marked by the black box. We use another colour scheme to highlight the seismic polarity of reflections of the seabed (B') and D (A'). PHAA – positive high amplitude anomalies, FGZ – free gas zone. (c) Inset of chimney 7. Six reflections (named as A–F) are picked to describe the amplitude variation around gas chimney and the result is shown in Fig. 4. PM – pockmark.

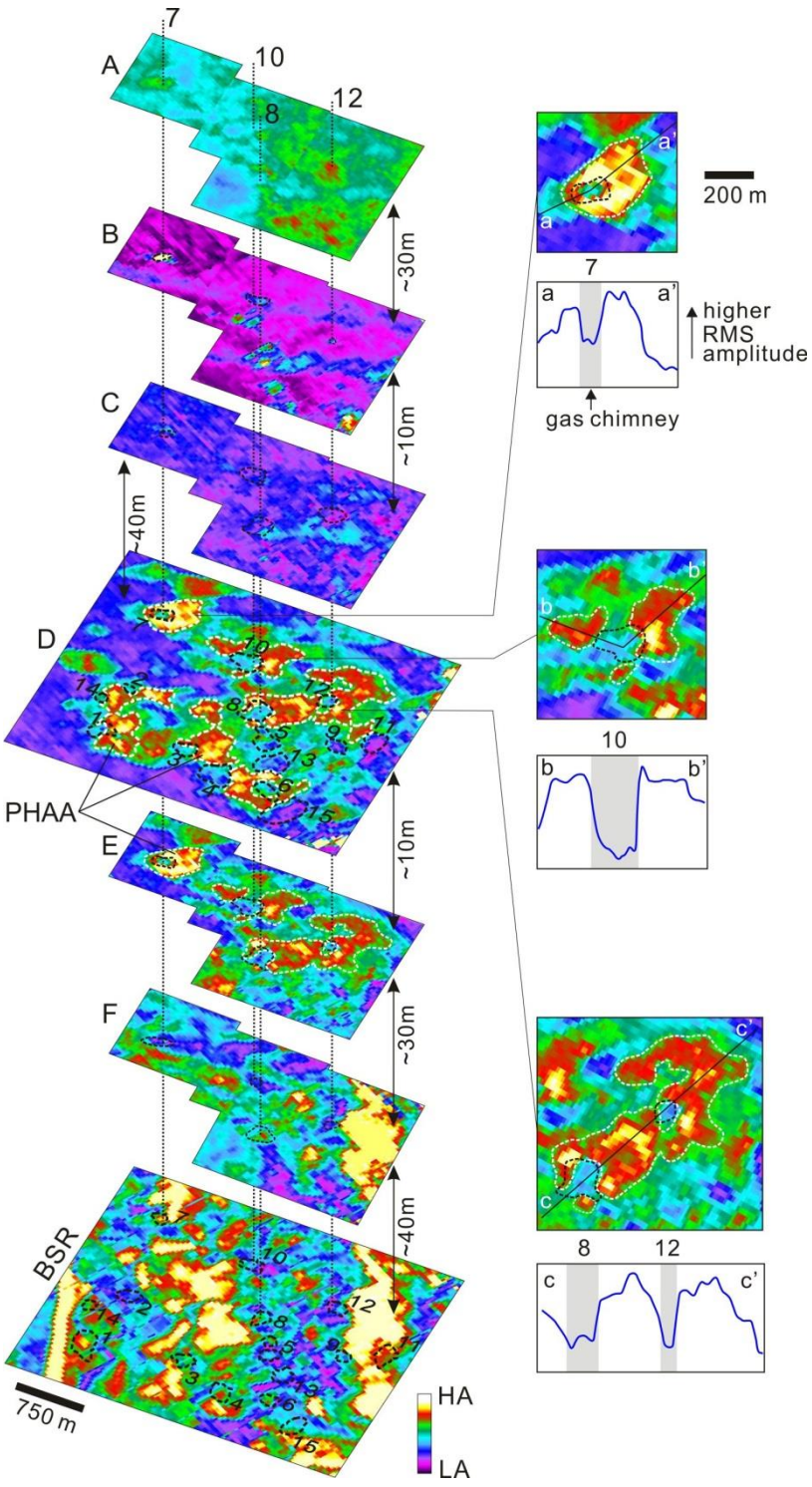

Fig.4 RMS amplitude map of the reflections A–F and the BSR (on the left). Their depths are marked in Fig. 3c. Vertical black dotted lines indicate the spatial location of chimneys 7, 8, 10 and 12. PHAAs at the reflection D and E (outlined by white dashed line) are identical and interpreted as hydrate deposits. Note that the amplitude values in the reflection A (the seabed) are very high and its colour scheme is different from others. The selected examples of the PHAAs are zoomed in (on the right).

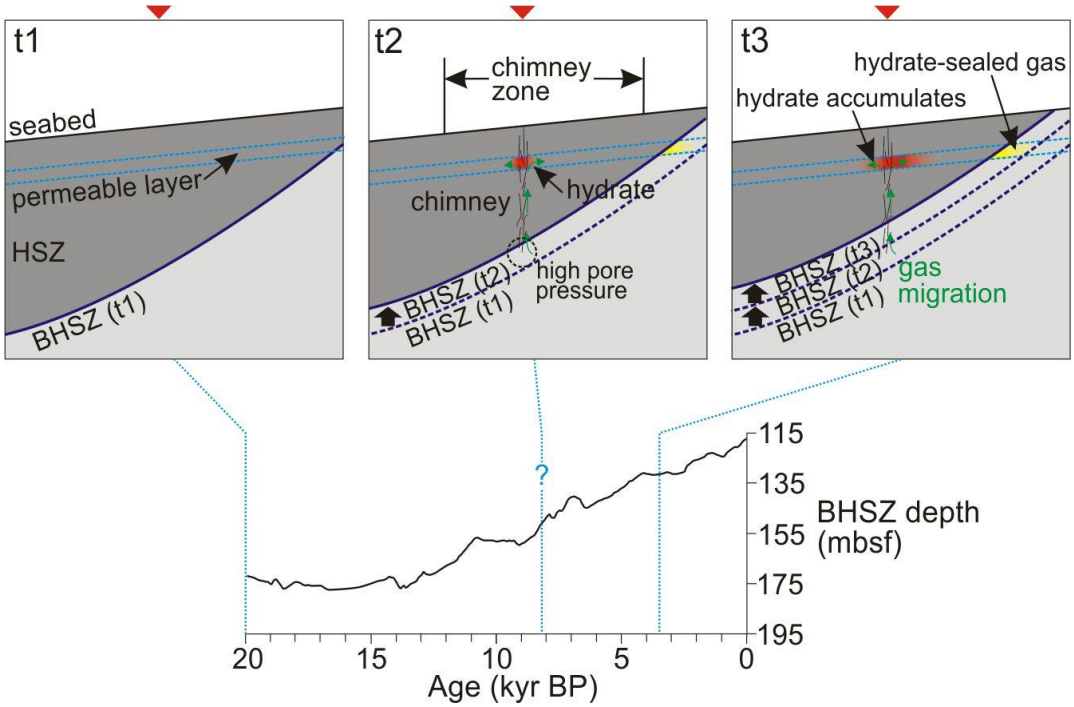

Fig.5 The modelling result of the BHSZ depth varying with time since the LGM. The snapshots at three timings (t1-t3) show how the hydrate deposit formed. The red triangle marks the location where the depth of the BHSZ is modelled in appendix.

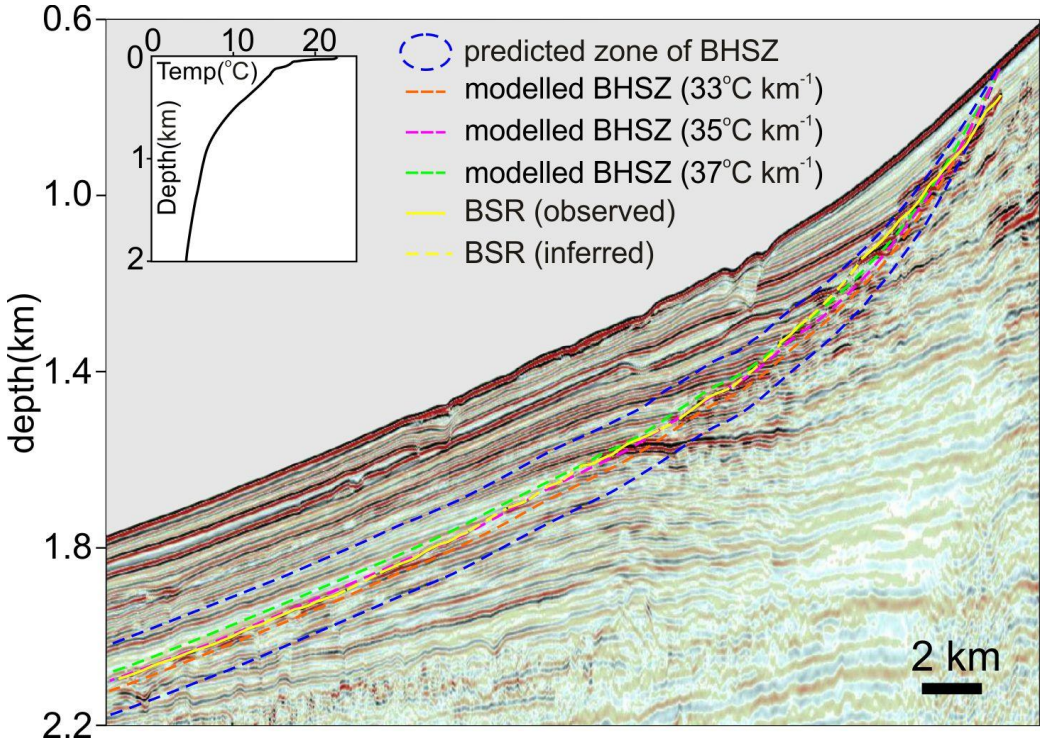

Fig. A.1 The modelled locations of the BHSZ with inputs of different geothermal gradient on a seismic cross section. Their correlation with the observed BSR determines the geothermal gradient. The averages of the vertical discrepancy between the observed and modelled BHSZ for the geothermal gradient of 33, 35 and 37 ^{o}C km^{-1} are 26.45, 10.81 and 18.49 m. The inset is the temperature-depth plot of the ocean water.

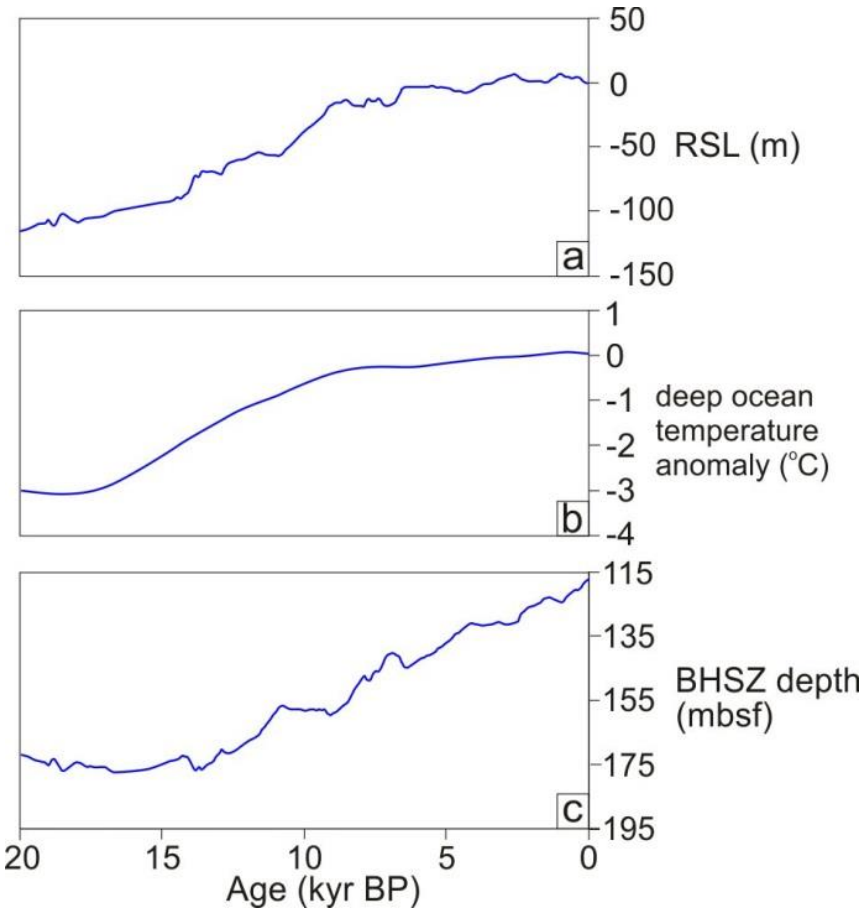

Fig. A.2 The variation of relative sea level (RSL) (a) and bottom water temperature (BWT) (b) in the last 20 kyr. The modelled depth of the BHSZ is shown in Fig. c. The site is marked by the red triangle in Fig. 5. A gas chimney is observed here. mbsf – metres below seafloor.